ADVANCED MATERIALS
www.advmat.de

Materials Views
www.MaterialsViews.com

# Element Specific Monolayer Depth Profiling

*Sebastian Macke, Abdullah Radi, Jorge E. Hamann-Borrero, Adriano Verna, Martin Bluschke, Sebastian Brück, Eberhard Goering, Ronny Sutarto, Feizhou He, Georg Cristiani, Meng Wu, Eva Benckiser, Hanns-Ulrich Habermeier, Gennady Logvenov, Nicolas Gauquelin, Gianluigi A. Botton, Adam P. Kajdos, Susanne Stemmer, George A. Sawatzky, Maurits W. Haverkort, Bernhard Keimer, and Vladimir Hinkov**

Sub-nanometer atomic layers buried underneath overlayers of different chemical composition play key roles in many areas of materials science and technology[1–5] – including as functional units in multilayer device structures,[6,7] seed layers for crystallization of thin films and nanostructures,[8] and buffer layers for strain relief or termination control.[9] The distribution of elements in and around buried layers often greatly affects their electronic phase behavior and functionality,[3,10–12] giving rise to rapidly growing demands for chemical diagnostics with atomic-scale resolution, element sensitivity and probing depths comparable to the dimensions of the device structures. Existing methods are either destructive (e.g., cross-sectional electron and scanning-probe spectroscopies)[13] or limited in probing depth and resolution (e.g., photoelectron spectroscopy).[14] Here we introduce a new analysis scheme for resonant X-ray reflectometry and demonstrate on the basis of experiments on two different metal-oxide heterostructures that this technique is capable of determining complex chemical composition profiles in a non-destructive manner, and with a probing depth of hundreds of nanometres, sub-nanometre spatial resolution, and an excellent elemental sensitivity. The technique thus has the potential to serve as an accurate and versatile characterization tool for nanostructures composed of complex materials.

The necessity for novel chemical diagnostics is particularly visible in the emerging field of nanostructured transition metal oxides (TMOs),[2–9] whose properties are highly sensitive to chemical composition and stoichiometry.[3,10–12] For instance, accurate information about the dopant-atom distribution is required to optimize the electron mobility in delta-doped TMO devices.[15,16] The current debate about the roles of chemical intermixing in driving metal-insulator transitions in TMO heterostructures further illustrates the need for diagnosis tools on the atomic scale.[3,10,11]

Established chemical profiling techniques satisfy some, but not all of the mentioned requirements. For example, X-ray absorption spectroscopy (XAS),[17] hard X-ray photoemission spectroscopy (HAXPES)[14] and ion-beam analysis[18] (SIMS and RBS) are element-specific but lack atomic-scale resolution. Scanning transmission electron microscopy in conjunction with electron energy loss spectroscopy (STEM-EELS)[13,19,20] does not have these limitations. However, the preparation procedure of the necessary thin cross-sectional slices is time-consuming, and (like SIMS) usually leads to destruction of the sample.

Here we introduce a new analysis scheme for resonant X-ray reflectivity (RXR), a complementary, nondestructive, element-specific spectroscopic probe of layered structures.[21,22] Despite its large probing depth and sub-nanometer resolution, the widespread application of RXR as a profiling tool has been hampered by difficulties in extracting quantitative information from

Dr. S. Macke, A. Radi, Dr. J. E. Hamann-Borrero, Dr. A. Verna, M. Bluschke, Prof. G. A. Sawatzky, Dr. M. W. Haverkort, Prof. V. Hinkov
Quantum Matter Institute and Department of Physics and Astronomy
University of British Columbia
2355 East Mall, Vancouver, V6T 1Z4, Canada
E-mail: hinkov@physik.uni-wuerzburg.de

Dr. S. Macke, Dr. A. Verna, G. Cristiani, M. Wu, Dr. E. Benckiser, Prof. H.-U. Habermeier, Dr. G. Logvenov, Dr. M. W. Haverkort, Prof. B. Keimer, Prof. V. Hinkov
Max Planck Institute for Solid State Research
Heisenbergstraße 1, 70569, Stuttgart, Germany

A. Radi
Department of Chemistry
University of British Columbia
2036 Main Mall, Vancouver, V6T 1Z1, Canada

Dr. J. E. Hamann-Borrero
Leibniz Institute for Solid State and Materials Research Dresden
Helmholtzstraße 20, 01069, Dresden, Germany

PD Dr. E. Goering
Max-Planck-Institute for Intelligent Systems
Heisenbergstraße 3, 70569, Stuttgart, Germany

Dr. R. Sutarto, Dr. F. He
Canadian Light Source, 44 Innovation Boulevard
Saskatoon, SK S7N 2V3, Canada

Dr. N. Gauquelin, Prof. G. A. Botton
Department of Materials Science and Engineering
McMaster University
1280 Main Street West, Hamilton, Ontario L845L8, Canada

Dr. A. P. Kajdos, Prof. S. Stemmer
University of California
Materials Research Laboratory
Santa Barbara, CA 93106–5121, U.S.A.

Dr. S. Brück, Prof. V. Hinkov
Physikalisches Institut und Röntgen Center for Complex Materials Systems (RCCM)
Universität Würzburg
Am Hubland, D-97074, Würzburg, Germany

DOI: 10.1002/adma.201402028


© 2014 WILEY-VCH Verlag GmbH & Co. KGaA, Weinheim

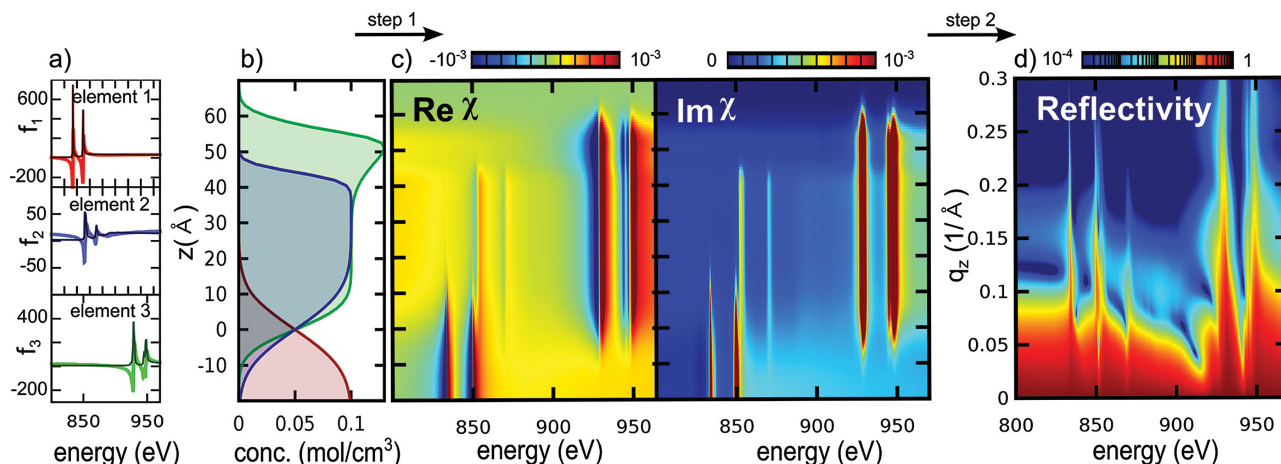


**Figure 1.** Schematic representation of the element specific method. (a) Real (light lines) and imaginary (dark lines) part of the scattering factors of three different elements; as a specific example, we use $La^{3+}$ (red), $Ni^{3+}$ (blue) and $Pr^{3+}$ (green). (b) Assumed chemical depth profile, i. e. molar concentration for each element. (c) In a first step, the depth profile of the real and imaginary parts of the susceptibility $\chi(z,\omega)$ are calculated. (d) In a second step, a reflectivity map is calculated. Subsequently, it is compared to a measured map, the chemical profile is adjusted and steps 1 and 2 are repeated, until convergence is achieved.

the complex interference patterns obtained in reflectivity. The scheme we have developed allows us to accurately reconstruct chemical profiles of layered samples with arbitrary complexity. We validate the method by comparing RXR results on TMO heterostructures with a-priori information, and with STEM-EELS measurements on the same samples.

In reflectivity[21] the material is described by the dielectric susceptibility $\chi(z,\omega)$, which depends on the concentration $c_i(z)$ and the individual atomic scattering factors $f_i(\omega)$ ($z$ is the distance from the substrate and $\omega$ is the photon frequency). The element, its valency and its electronic properties are characterized by the unique frequency dependence of $f_i(\omega)$ (resonant absorption edge, **Figure 1**(a)). The main problem is that phase information is lost during the measurement process, which prohibits a direct inversion of the **q** (wavevector) resolved data into spatially resolved information.[21,23–25] Most reflectivity investigations thus far have focused on measurements at a single, non-resonant energy, typically in the hard X-ray range, which only provides information about the overall electron concentration, without referring to individual elements. For this limited case, or for the related problem in neutron reflectivity, ways to solve or at least circumvent the phase problem[24] have been put forward, for instance by introducing a reference layer into the heterostructure.[26]

Another approach, first discussed in Reference [27] for the magnetic properties of Fe, is to take advantage of the strong variation of $\chi(\omega)$ in the vicinity of resonant absorption edges. Later endeavours to perform chemical profiling this way were either aiming at one single element,[28,29] or were limited by the small number of measured energies or the restricted wave vector range.[30,31]

Here we extend the scope of RXR by exploiting the full potential of this approach, which not only resolves the inherent element nonspecificity of non-resonant reflectometry: Also, the particular frequency dependence of $\chi(\omega)$, the interference character of the measurements and the Kramers-Kronig relations, which relate the real and imaginary part of $\chi(z,\omega)$, preserve phase information in sufficiently large (**q**, $\omega$) maps such as those we have measured (Figure 3). This allows us to reconstruct the detailed chemical profile.

To capture arbitrary intermixing and non-stoichiometry, we start on the elemental level by describing the sample using atomic scattering factors $f_i(\omega)$ and the concentration depth profiles $c_i(z)$ of each individual element in each of the valencies present in the sample (Figure 1(b)). Figure 1(c) exemplifies how the individual scattering factors shown in Figure 1(a) add up to yield the real and imaginary part of $\chi(z,\omega)$. The total depth-resolved susceptibility is

$$\chi(z,\omega)=\frac{4\pi}{|k_0|^2}r_{el}\sum_i N_A c_i(z)f_i(\omega)$$

where $\mathbf{k}_0$ is the wave vector of the incoming beam, $N_A$ the Avogadro constant, and $r_{el}$ is the classical electron radius; $f_i$ is obtained from XAS as described in the experimental section. Gradients are modeled by segmentation[24] into thin layers with constant $c_i(z)$ to allow the calculation of the resulting reflectivity according to the Parratt formalism[32] as exemplified in Figure 1(d). The remaining free parameters, namely the segment concentrations and thicknesses, are optimized in a simultaneous fit to all measured reflectivity curves first using genetic and annealing algorithms to avoid getting trapped in deep local minima, followed by least-squares fits to obtain the final results.[24,33]

We demonstrate our new approach using two different systems of topical interest: (i) Structurally nearly perfect $SrTiO_3$ (STO) films, $\delta$-doped with La. Samples of this type have recently been used to obtain two-dimensional electron gases with very high mobility.[15,16] We use such a sample to determine the detection limit for the concentration of dilute elements in buried layers. (ii) A $PrNiO_3$ (PNO) thin film, a member of a class of compounds that has recently attracted considerable attention because its phase behaviour can be controlled in heterostructures.[5,34,35] This sample reveals the full power of the method to determine complex chemical profiles since


© 2014 WILEY-VCH Verlag GmbH & Co. KGaA, Weinheim

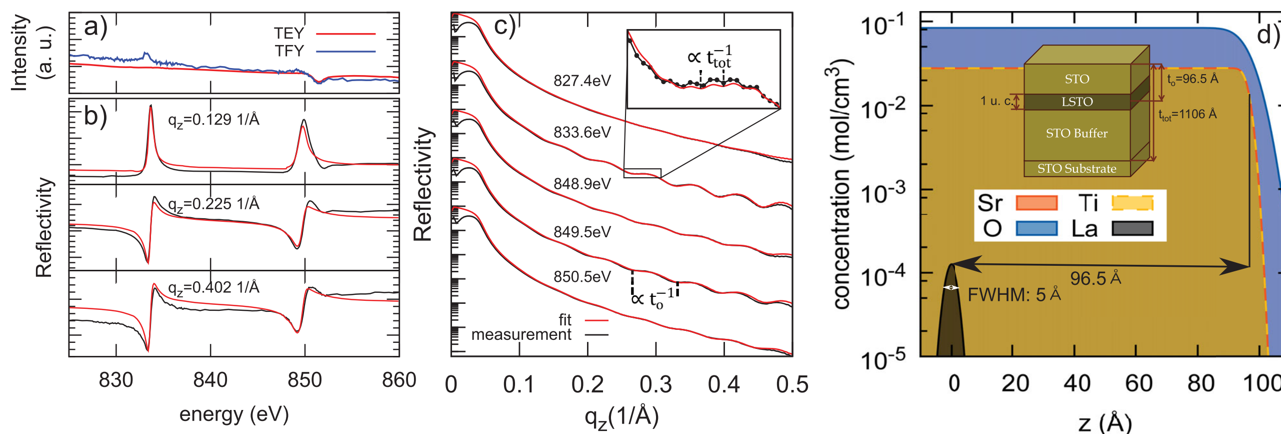


**Figure 2.** $SrTiO_3$ sample δ-doped with Lanthanum. (a) XAS data around the La $M_5$ and $M_4$ edges in total electron yield (TEY) and fluorescence yield (FY) mode. (b) Constant-$q$ reflectivity scans, measured within the same energy range as the data in a), and compared with fitted simulations. (c) Constant-energy reflectivity scans, compared with fitted simulations. For clarity, the curves have been multiplied by a factor of 100 with respect to each other. The two vertical lines mark the oscillations stemming from the STO overlayer. The inset shows a magnified view of the curve, exposing thickness fringes stemming from the STO buffer layer, which are marked by vertical lines. (d) Corresponding concentration profile, encompassing the surface and the buried $La_xSr_{1-x}TiO_3$ layer, obtained from the fits to the data. The resulting fitted parameters are: $x = 0.006$ and $t_0 = (96 \pm 1)$ Å, and the total thickness of the synthesized heterostructure, including the buffer layer, is $t_{tot} = (1106 \pm 10)$ Å. The inset schematically shows the structure of the entire sample.

the unprotected film surface underwent substantial chemical modification.

A titanate heterostructure, $SrTiO_3/La_xSr_{1-x}TiO_3$ (LSTO, 1 monolayer)/$SrTiO_3$ (buffer)//$SrTiO_3$ (001) with a nominal La content of $x = 0.005$ was grown using molecular beam epitaxy (see experimental section). The thickness $t_o$ of the top STO layer was not known to the RXR team. Furthermore, an STO buffer of unspecified thickness was grown below the LSTO layer, resulting in a total thickness of $t_{tot}$.

We investigated the sample with XAS and RXR (**Figure 2**). Even in the more bulk-sensitive FY mode the XAS peaks barely exceed the noise level, and besides, XAS even in principle does not allow a quantitative assessment of either $x$ or $t_o$. The RXR data, on the other hand, allow the precise determination of $x$ and $t_o$: A first estimate of $t_o$ can be obtained from the large thickness oscillations visible in panel (c). From the comparison of the various scans taken at and around the La edge with simulations based on the model in panel (d), which resulted from the fitting procedure described above, we obtain $x = 0.006$ and an STO layer thickness of $t_o = (96 \pm 1)$ Å, in close agreement with the targeted $x = 0.005$ and 100 Å. We remark that, considering the large signal-to-noise ratio of the constant-$q$ data in Figure 2, the method has the potential to detect elemental concentrations significantly below the concentration of $x = 0.006$ found in our sample.

The total thickness $t_{tot}$ of the structure, including the STO buffer layer, was extracted from the small dense oscillations visible in the inset of panel (c). These result from additional elemental contrast provided by tiny amounts of organic compounds on the substrate surface, which cannot be fully removed when preparing it for the film deposition.[36]

The second sample is $PrNiO_3$ deposited by pulsed laser epitaxy on $(LaAlO_3)_{0.3}$-$(Sr_2AlTaO_6)_{0.7}$ substrate with (100) termination (see experimental section). While the targeted thickness was 10 nm, measurements at the Ni L-edge indicate a thickness closer to ≈9 nm. To resolve this seeming contradiction, we have performed comprehensive RXR mappings around the Ni $L$- and Pr $M$-edges, complemented by individual measurements close to the O $K$-edge and at intermediate energies (**Figure 3**). To obtain the detailed chemical profile, we assumed a model consisting of a stoichiometric $PrNiO_3$ layer of variable thickness and roughness, beginning at the substrate, covered by a layer in which the concentrations, thicknesses and roughnesses of the Pr, Ni and O distributions were all variable and independent from each other. This model allows us to capture any potential intermixing at the substrate-film interface and non-stoichiometry at the film surface, while at the same time keeping the number of free parameters manageable (see Supporting Information and Figure S2).

The fitted individual Pr, Ni and O concentration profiles and the corresponding parameters are shown in **Figure 4**(b). The simulated RXR results based on these profiles are in excellent agreement with the measured data (Figure 3). The concentration profile in Figure 4(b) has several remarkable features: First, at the surface of the film there is a region in which the Ni concentration goes to zero whereas the Pr concentration is still substantial and only vanishes nearly two unit cells above. The resulting full widths at half maximum of the Ni and Pr distributions are 91.6 Å and 97.6 Å, respectively, both with a roughness of about 2 Å. Stoichiometric variations of this kind can drastically affect the electronic properties of transition metal oxides, and are especially important for the interpretation of data from surface-sensitive techniques.

Second, there is a thick contamination layer consisting of oxygen and lighter elements on top of the film, which did not desorb in UHV. Taking into account this layer is crucial to obtain a satisfactory fit even at the relatively distant Ni and Pr edges due to the additive character and Kramers-Kronig consistency of $\chi(z,\omega)$. We refrain from a detailed determination of its composition, which would require substantial additional mapping at energies below the oxygen $K$-edge, without adding new information about the actual film.


© 2014 WILEY-VCH Verlag GmbH & Co. KGaA, Weinheim

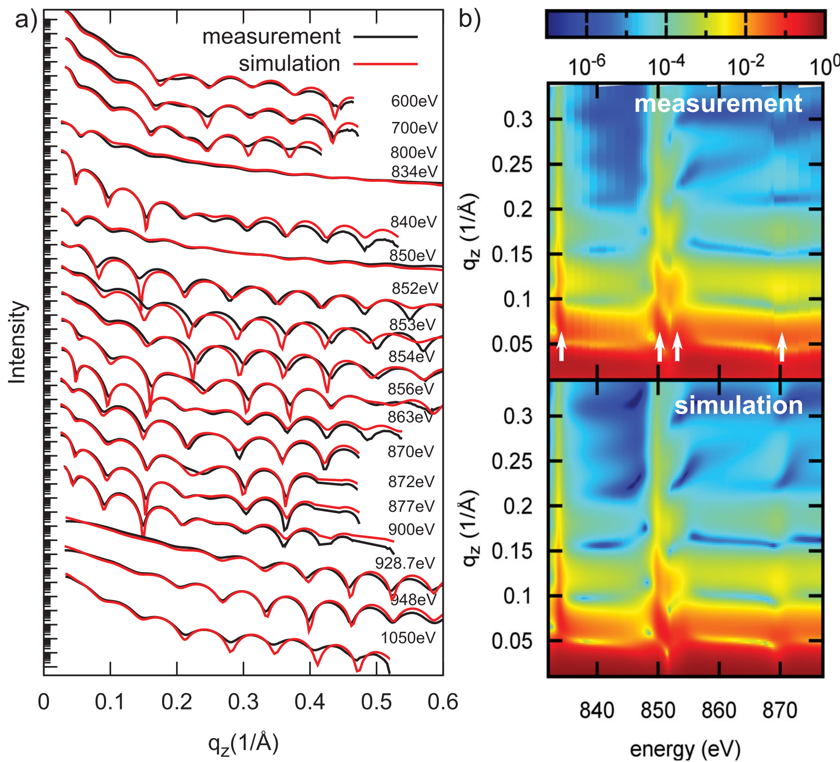


**Figure 3.** RXR results on the $PrNiO_3$ film. (a) Representative measured (red lines) and fitted (black lines) reflectivity scans. (b) Comparison between the measured and the fitted reflectivity map comprising a total of 31 individual scans, including those shown in a). The energies of the four resonances La $M_5$, La $M_4$, Ni $L_3$ and Ni $L_2$ are marked with arrows.

Third, the roughness at the substrate interface is below the detection limit, indicating that $PrNiO_3$ grows well on $(LaAlO_3)_{0.3}$-$(Sr_2AlTaO_6)_{0.7}$.

We tested the robustness and consistency of our results in numerous ways. Qualitative changes of the model like moving the Ni-depleted region from the surface to the substrate interface lead to unsolvable inconsistencies in the fit. Also, irrespective of the assumed initial configuration, the genetic algorithm, which inherently probes a wide range of possible solutions, including such without a Ni depletion layer, without an organic contamination layer, and with a Pr/Ni ratio unequal one, always approached our final solution (Figure 4(b)). We further point out that the influence of the three major parameters characterizing each layer on the reflectivity profiles is quite different from each other (Figure S3): The thickness is correlated to the thickness fringe periodicity of the reflectivity profiles but not to the intensity, whereas the concentration affects the intensity at all wave vectors and the roughness mainly affects the thickness fringe amplitude and intensity at large wave vector transfers, but both do not affect the fringe periodicity. Therefore, errors in the determination of one of the parameters cannot be compensated by

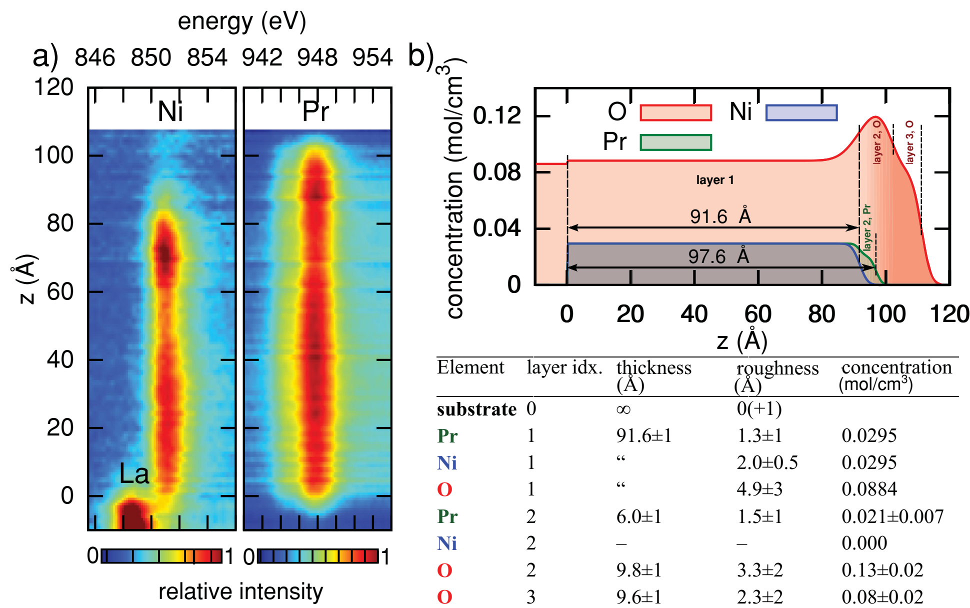


| Element | layer idx. | thickness (Å) | roughness (Å) | concentration (mol/cm$^3$) |
|---|---|---|---|---|
| **substrate** | 0 | ∞ | 0(+1) | |
| **Pr** | 1 | 91.6±1 | 1.3±1 | 0.0295 |
| **Ni** | 1 | " | 2.0±0.5 | 0.0295 |
| **O** | 1 | " | 4.9±3 | 0.0884 |
| **Pr** | 2 | 6.0±1 | 1.5±1 | 0.021±0.007 |
| **Ni** | 2 | – | – | 0.000 |
| **O** | 2 | 9.8±1 | 3.3±2 | 0.13±0.02 |
| **O** | 3 | 9.6±1 | 2.3±2 | 0.08±0.02 |

**Figure 4.** Comparison between EELS and RXR results on the $PrNiO_3$ film. (a), Representative EELS profile around the Pr $M_4$ and Ni $L_3$ edges. The same constant background was subtracted for both profiles. For each panel, the color scale was chosen such that the maximal intensity at the corresponding edge is dark red. (b), Elemental depth profile for the three elements present in the film, Pr, Ni, and O, obtained from fits to the RXR data shown in Figure 3. The region at the surface marked with darker red contains other light elements such as carbon and hydrogen, in addition to oxygen. The three layers into which the sample was subdivided for the analysis are marked with vertical lines. The table shows the fitting results for the thickness, roughness and concentration characterizing the profile of each element in the corresponding layer. Roughnesses are valid for the top interface of the corresponding layer. Note that in the element-specific method, not all elements are present in all layers, and thicknesses can be different within the same layer.


© 2014 WILEY-VCH Verlag GmbH & Co. KGaA, Weinheim

modifications in another one. Correlations between the three parameters are thus minimal, and all of them can be robustly extracted from the fits.

We completed our study by performing complementary STEM-EELS measurements on specimens extracted from various locations on the $PrNiO_3$ sample. Representative data around the Ni and Pr edges is shown in Figure 4(a) and contrasted with the profile derived from the RXR measurements. It corroborates our finding of a heavily Ni depleted surface layer and substantial chemical roughness. The atomic-resolution data in Supporting Figures S4 and S5 is also consistent with our RXR finding of a sharp substrate/film interface. The full width half maximum of the Ni profile, averaged over the different EELS measurements, is 88.5 Å, in remarkable agreement with the RXR result of 91.6 Å. The same holds for Pr (97.6 Å vs. 103 Å).

The two methods are complementary in different aspects: RXR is a non-destructive scattering technique, whose in-plane resolution is limited by the macroscopic beam size (in present implementations µm and above). STEM-EELS is destructive, but offers sub-nm resolution in one in-plane direction. Whereas both exhibit monolayer or close-to monolayer depth resolution, degraded crystallinity in the Ni-depleted layer might effectively deteriorate resolution for STEM-EELS, but it does not impact RXR results. The time and effort involved is comparable: Advance application for measurement time is necessary for both, and STEM requires an elaborate specimen preparation, whereas RXR depends on a sophisticated data analysis.

We next compare our approach to further established methods with respect to destructiveness, the elemental detection limit, depth resolution and everyday availability. Several methods such as SIMS,[37] Rutherford backscattering (RBS),[18] and sputtering XPS (SXPS)[38] can detect elemental densities of 100 p.p.m. or below, and in contrast to the more sophisticated STEM-EELS and RXR are frequently available in local laboratories. They are thus very good tools for quick routine characterization immediately after sample growth or processing. However, many of them have the disadvantage of being destructive, thus potentially disturbing the stoichiometry with respect to volatile elements like oxygen. Depth resolution is a further critical parameter: while several nanometers are readily achievable, sub-nm or monolayer resolution is limited to a few techniques such as RXR and STEM-EELS. Standing-wave techniques are powerful non-destructive, element specific methods, which exhibit monolayer resolution, but have a limited scope since they require nearly perfect interfaces[39] or elaborate superlattice samples.[40]

Consequently, RXR will be typically applied to selected samples which have undergone preliminary characterization with lab-based techniques. In this work we have focused our analysis on the determination of the chemical composition profile of heterostructures. The capability of RXR to extract information about interfacial electronic,[41,42] magnetic,[43] and orbital[44] reconstruction in structurally and chemically nearly perfect samples with simple, judiciously chosen layer sequences has been previously demonstrated. The next step is the extension of our approach to such reconstruction phenomena in systems of increasing chemical and physical complexity: It is a powerful method to study the chemical and physical properties of heterostructures comprising functional materials such as transition-metal oxides, topological insulators or pnictide superconductors. Technical developments are underway to allow measurements with a strongly reduced beam spot size in the nanometre range, thus extending its applicability to laterally structured multilayers, ultimately allowing the spectro-microscopic investigation of novel devices.

## Experimental Section

The $SrTiO_3$ heterostructures, $\delta$-doped with La, were grown using a hybrid molecular beam epitaxy (MBE) approach,[36] similar to that used for the films investigated in Reference [16], at a substrate temperature of 900 °C (measured by thermocouple). Oxygen was supplied during growth using a RF plasma source operating at 250 W with an oxygen background pressure of $4\cdot10^{-6}$ Torr. After growth, these films were annealed in a rapid thermal annealing furnace in 1 atm of oxygen at 800 °C for 30 s to backfill any oxygen vacancies generated during growth.

The $PrNiO_3$ samples were synthesized using pulsed laser deposition (PLD). Starting materials were ablated using a KrF excimer laser (240 nm) with 2 Hz pulse rate and 1.6 J/cm$^2$ energy density, and deposited in 0.5 mbar oxygen atmosphere at 730 °C. The resulting films were subsequently annealed in 1 bar oxygen atmosphere at 690 °C for 30 min. The out-of-plane lattice constant of the $PrNiO_3$ film was determined from X-ray diffraction to be (3.780 ± 0.005) Å.

The XAS and X-ray reflectivity measurements were carried out using a 4-circle in-vacuum diffractometer at the REIXS 101D-2 beamline of the Canadian Light Source (CLS) in Saskatoon, Canada. The samples were mounted with their surface normal in the scattering plane. The measurements were performed using $\sigma$-polarized light. The reflectivity scans were performed in specular geometry, in which the incident angle $\theta$ is defined relative to the surface plane. Scans were recorded and analyzed up to a detector angle of $2\theta \approx 90°$, and where signal-to-noise ratio permitted up to 110°. The temperature was kept constant at 298 K. A detailed description of the experimental setup is reported in Reference [44].

The off-resonant parts of the atomic scattering factors of La, Pr, Ni, Ti, and O were taken from Chantler tables.[45] The corresponding resonant parts were retrieved from XAS measurements in total electron yield (TEY) mode, background corrected, and aligned with the Chantler database as described in Reference [4]. To correct the distortion of the La signal due to the significant self-absorption, its scattering factor was additionally parameterized and fitted to reflectivity data. The resulting imaginary part of the scattering factors of the above elements is shown in Figure S1. The other elements present in our systems (Sr, Al, Ta) were taken into account by using tabulated values only, since their absorption edges are sufficiently far away in energy as to not interact appreciably with the main elements. For all elements, the real part of the scattering factors was obtained by Kramers-Kronig transformation. The RXR analysis method discussed in this paper is implemented in the software package ReMagX,[46] www.remagx.org.

STEM and EELS measurements were carried out on a FEI Titan3 microscope at an acceleration voltage of 200 kV. A FIB sample was prepared and further thinned at liquid nitrogen temperature until a thickness of around 50 nm was reached. EELS acquisitions were performed with an energy resolution of 0.7 eV at a dispersion of 0.1 eV per pixel on a GIF Tridiem ERS. The spectrum images were acquired with a spacing 0.5 Å/pixel and 50 ms/pixel acquisition time. The convergence angle and collection angle used for the experiment were 20 and 200 mrad, respectively.

## Supporting Information

Supporting Information is available from the Wiley Online Library or from the author.


© 2014 WILEY-VCH Verlag GmbH & Co. KGaA, Weinheim

## Acknowledgements

The work was supported by the German Research Foundation under grant TRR80, proj. C1, by the Canadian organizations NSERC, CFI, CIFAR, and CRC and by the German Max-Planck Society. Parts of the research were performed at the Max-Planck-UBC Centre for Quantum Materials. Parts of the research was performed at the Canadian Light Source, which is funded by the Canada Foundation for Innovation, the Natural Sciences and Engineering Research Council of Canada, the National Research Council Canada, the Canadian Institutes of Health Research, the Government of Saskatchewan, Western Economic Diversification Canada, and the University of Saskatchewan. Work at UCSB was supported by the UCSB MRL, which is supported by the MRSEC Program of the National Science Foundation under Award No. DMR-1121053. A.P.K. received support from the National Science Foundation through a Graduate Research Fellowship (Grant No. DGE-1144085). The electron microscopy and EELS was carried out at the Canadian Centre for Electron Microscopy, a National Facility supported by NSERC and McMaster University. G. A. B. is grateful to NSERC for a Discovery Grant.
Note: The author name Adriano Verna was added to the author list on September 23, 2014.

Received: May 6, 2014
Revised: June 25, 2014
Published online: August 8, 2014

[1] H. Y. Hwang, Y. Iwasa, M. Kawasaki, B. Keimer, N. Nagaosa, Y. Tokura, *Nat. Mat.* **2012**, *11*, 103.
[2] A. Ohtomo, H. Hwang, *Nature* **2004**, *427*, 423.
[3] A. Gozar, G. Logvenov, L. Fitting Kourkoutis, A. T. Bollinger, L. A. Giannuzzi, D. A. Muller, I. Bozovic, *Nature* **2008**, *455*, 782.
[4] E. Benckiser, M. Haverkort, S. Brück, E. Goering, S. Macke, A. Fraño, X. Yang, O. Andersen, G. Cristiani, H. Habermeier, et al. *Nat. Mat.* **2011**, *10*, 189.
[5] M. Gibert, P. Zubko, R. Scherwitzl, J. Íñiguez, J.-M. Triscone, *Nat. Mat.* **2012**, *11*, 195.
[6] C. Cen, S. Thiel, J. Mannhart, J. Levy, *Science* **2009**, *323*, 1026.
[7] J. T. Ye, S. Inoue, K. Kobayashi, Y. Kasahara, H. T. Yuan, H. Shimotani, Y. Iwasa, *Nat. Mat.* **2010**, *9*, 125.
[8] M. Li, X. Jiang, G. Samant, C. Felser, S. S. P. Parkin, *Appl. Phys. Lett.* **2013**, *103*, 032410.
[9] W. S. Choi, J.-H. Kwon, H. Jeen, J. E. Hamann-Borrero, A. Radi, S. Macke, R. Sutarto, F. He, G. A. Sawatzky, V. Hinkov, M. Kim, H. N. Lee, *Nano Lett.* **2012**, *12*, 4966.
[10] N. Nakagawa, H. Y. Hwang, D. A. Muller, *Nat. Mat.* **2006**, *5*, 204.
[11] W. Siemons, G. Koster, H. Yamamoto, W. A. Harrison, G. Lucovsky, T. H. Geballe, D. H. A. Blank, M. R. Beasley, *Phys. Rev. Lett.* **2007**, *98*, 196802.
[12] M. P. Warusawithana, C. Richter, J. A. Mundy, P. Roy, J. Ludwig, S. Paetel, T. Heeg, A. A. Pawlicki, L. F. Kourkoutis, M. Zheng, M. Lee, B. Mulcahy, Y. Zander, W. Zhu, J. Schubert, J. N. Eckstein, D. A. Muller, C. S. Hellberg, J. Mannhart, D. G. Schlom, *Nat. Comm.* **2013**, *4*, 2351.
[13] R. Egerton, *Electron energy-loss spectroscopy in the electron microscope*, DOI:10.1007/978-1-4419-9583-4-1, Springer, **2011**.
[14] J. Rubio-Zuazo, G. Castro, *Journal of Physics: Conference Series* **2008**, *100*, 012042.
[15] Y. Kozuka, M. Kim, C. Bell, B. Kim, Y. Hikita, H. Hwang, *Nature* **2009**, *462*, 487.
[16] B. Jalan, S. Stemmer, S. Mack, S. J. Allen, *Phys. Rev. B* **2010**, *82*, 081103.
[17] J. Stöhr, H. C. Siegmann, *Magnetism – From fundamentals to nanoscale dynamics*, ISBN:978-3-540-30283-4, Springer, **2006**.
[18] C. Jeynes, R. P. Webb, A. Lohstroh, *Rev. Accl. Sci. Tech.* **2011**, *4*, 41.
[19] G. A. Botton, *MRS Bull.* **2012**, *37*, 21.
[20] D. A. Muller, *Nat. Mat.* **2009**, *8*, 263.
[21] J. Als-Nielsen, D. McMorrow, *Elements of modern X-ray physics*, ISBN:978-0470973943, Wiley, **2011**.
[22] J. Fink, E. Schierle, E. Weschke, J. Geck, *Reports on Progress in Physics* **2013**, *76*, 056502.
[23] K. Zimmermann, M. Tolan, R. Weber, J. Stettner, A. Doerr, W. Press, *Phys. Rev. B* **2000**, *62*, 10377.
[24] A. Van DerLee, F. Salah, B. Harzallah, *J. Appl. Cryst.* **2007**, *40*, 820.
[25] T. Hohage, K. Giewekemeyer, T. Salditt, *Phys. Rev. E* **2008**, *77*, 051604.
[26] C. F. Majkrzak, N. F. Berk, *Phys. Rev. B* **1995**, *52*, 10827.
[27] C. Kao, J. B. Hastings, E. D. Johnson, D. P. Siddons, G. C. Smith, G. A. Prinz, *Phys. Rev. Lett.* **1990**, *65*, 373.
[28] P. Abbamonte, L. Venema, A. Rusydi, G. A. Sawatzky, G. Logvenov, I. Bozovic, *Science* **2002**, *297*, 581.
[29] C. Park, P. Fenter, *J. Appl. Cryst.* **2007**, *40*, 290.
[30] J. Bai, M. Tomkiewicz, P. Montano, *Z. Phys. B* **1995**, *97*, 465.
[31] D. Kim, H. Lee, S. Kim, H. Kang, D. Noh, H. Kim, S. Sinha, *Appl. Phys. Lett.* **2004**, *85*, 6427.
[32] L. Parratt, *Phys. Rev.* **1954**, *95*, 359.
[33] W. Press, B. Flannery, S. Teukolsky, W. Vetterling, et al. *Numerical recipes*, ISBN:978-0521880688, Cambridge Univ Press, **1986**.
[34] A. Boris, Y. Matiks, E. Benckiser, A. Frano, P. Popovich, V. Hinkov, P. Wochner, M. Castro-Colin, E. Detemple, V. Malik, et al. *Science* **2011**, *332*, 937.
[35] A. Frano, E. Schierle, M. W. Haverkort, Y. Lu, M. Wu, S. Blanco-Canosa, U. Nwankwo, A. V. Boris, P. Wochner, G. Cristiani, H. U. Habermeier, G. Logvenov, V. Hinkov, E. Benckiser, E. Weschke, B. Keimer, *Phys. Rev. Lett.* **2013**, *111*, 106804.
[36] B. Jalan, J. Cagnon, T. Mates, S. Stemmer, *J. Vac. Sci. Technol. A* **2009**, *27*, 1365.
[37] S. Hofmann, *Phil. Trans. R. Soc. Lond. A* **2004**, *362*, 55.
[38] D. Briggs, M. P. Seah, *Practical surface analysis by Auger and X-ray photoelectron spectroscopy*, ISBN: 9780471262794, Wiley, New York, **1983**.
[39] N. Nakanishi, H. Hashizume, T. Terashima, Y. Bando, O. Michikami, S. Maeyama, M. Oshima, *Phys. Rev. B* **1993**, *48*, 10524.
[40] A. X. Gray, C. Papp, B. Balke, S.-H. Yang, M. Huijben, E. Rotenberg, A. Bostwick, S. Ueda, Y. Yamashita, K. Kobayashi, E. Gullikson, J. B. Kortright, F. M. F. de Groot, G. Rijnders, D. H. A. Blank, R. Ramesh, C. S. Fadley, *Phys. Rev. B* **2010**, *82*, 205116.
[41] Ş. Smadici, P. Abbamonte, A. Bhattacharya, X. Zhai, B. Jiang, A. Rusydi, J. N. Eckstein, S. D. Bader, J.-M. Zuo, *Phys. Rev. Lett.* **2007**, *99*, 196404.
[42] H. Wadati, D. G. Hawthorn, J. Geck, T. Higuchi, Y. Hikita, H. Y. Hwang, L. Fitting Kourkoutis, D. A. Muller, S.-W. Huang, D. J. Huang, H.-J. Lin, C. Schüßler-Langeheine, H.-H. Wu, E. Schierle, E. Weschke, N. J. C. Ingle, G. A. Sawatzky, *J. Appl. Phys.* **2009**, *106*, 083705.
[43] J. M. Tonnerre, M. De Santis, S. Grenier, H. Tolentino, V. Langlais, E. Bontempi, M. Garcia-Fernandez, U. Staub, *Phys. Rev. Lett.* **2008**, *100*, 157202.
[44] D. G. Hawthorn, F. He, L. Venema, H. Davis, A. J. Achkar, J. Zhang, R. Sutarto, H. Wadati, A. Radi, T. Wilson, G. Wright, K. M. Shen, J. Geck, H. Zhang, V. Novak, G. A. Sawatzky, *Rev. Sci. Instrum.* **2011**, *82*, 073104.
[45] C. Chantler, *Journal of Physical and Chemical Reference Data* **1995**, *24*, 71.
[46] S. Macke, E. Benckiser, E. Goering, V. Hinkov, ReMagX – X-ray magnetic reflectivity tool. Max Planck – UBC centre for quantum materials. URL www.remagx.org.


© 2014 WILEY-VCH Verlag GmbH & Co. KGaA, Weinheim